LIMNOLOGY
and
OCEANOGRAPHY: METHODS

ASLO

Limnol. Oceanogr.: Methods 15, 2017, 897–902

doi: 10.1002/lom3.10209

Pressure correction for the computation of nitrate concentrations in seawater using an in situ ultraviolet spectrophotometer

Carole M. Sakamoto ,* Kenneth S. Johnson , Luke J. Coletti, Hans W. Jannasch
Monterey Bay Aquarium Research Institute, Moss Landing, California

Abstract

The most accurate calculation of nitrate concentration from the ultraviolet (UV) absorption spectrum of seawater requires that the absorption signal due to bromide in seawater be removed before nitrate concentrations are computed. Recent work suggests that the UV absorption spectrum of bromide in seawater has a pressure dependence. Neglect of this signal could add a bias when nitrate concentrations at high pressure are computed from UV measurements. Laboratory tests were conducted to determine the pressure dependence of the bromide absorption in seawater. Our results confirm the existence of a pressure coefficient in the bromide spectrum. The percentage change in bromide molar absorptivity is wavelength and temperature independent. The effect of pressure on the absorptivity of sea salt (E_{SW}), which is dominated by bromide ion, can therefore be calculated as $E_{SW\,pressure} = E_{SW\,1\,dbar} * (1 - 0.026 * \text{Pressure (dbar)}/1000)$ The correction amounts to an error of around 0.95 μM nitrate at 1000 dbar. The pressure correction should be used in the calculations of nitrate concentrations from UV absorption spectra at high pressures.

Johnson and Coletti (2002) reported the development of an in situ ultraviolet spectrophotometer (ISUS) instrument that could directly measure nitrate in the aquatic environment with short response time (< 1 s) and low power requirements. There is now widespread use of ultraviolet (UV) optical instruments for measuring nitrate in rivers (Pellerin et al. 2009; Aubert and Breuer 2016), turbid coastal waters (Zielinski et al. 2011; Frank et al. 2014), moorings (Collins et al. 2013; Woodgate et al. 2015), and autonomous underwater vehicles (AUVs) (Johnson and Needoba 2008; Harvey et al. 2012).

With the advent of pressure tolerant optics, both the ISUS and the closely related Submersible UV Nitrate Analyzer (SUNA) (MacIntyre et al. 2009) are now regularly being used to measure nitrate profiles to depths of 2000 m while mounted on profiling floats (Johnson et al. 2010; Johnson et al. 2013; D'Ortenzio et al. 2014; Pasqueron de Fommervault et al. 2015). The number of profiles being made to depths of 1000 m or more now on Biogeochemical-Argo floats greatly exceeds the number of profiles made by laboratory analyses on samples collected by ships and reported to the US National Oceanographic Data Center (Johnson et al. 2017). The nitrate data from profiling floats is quality controlled by comparing the concentrations at depths greater than 1000 m with models based on historical bottle data so increased accuracy at high pressures is paramount.

The algorithm to compute nitrate reported by Johnson and Coletti (2002) was updated (Sakamoto et al. 2009) to account for a temperature dependence of the bromide light absorption spectrum. In a recent study using UV nitrate sensors on profiling floats in the Mediterranean Sea, Pasqueron de Fommervault et al. (2015) suggested that there is also a pressure coefficient to the UV light absorption spectrum of bromide. They estimated the pressure correction was −2% per 1000 dbar based on an empirical correction using the measured nitrate profiles and a dedicated test with the nitrate sensor in a closed Niskin bottle that was sent to depth.

This study was conducted to confirm the existence of a pressure dependence on the bromide absorption and to quantify the form of the pressure correction factor for nitrate measurements using UV optical sensors. Measurements were made using a temperature controlled pressure chamber in the laboratory.

Materials and procedures

The UV light absorption spectrum of seawater was measured in a titanium pressure vessel fitted with the optics of an ISUS nitrate sensor (Fig. 1). The pressure vessel is lined with polyether ether ketone (PEEK). Pressure was applied with a Teledyne ISCO Model 260D Syringe Pump and measured with a high precision pressure transducer (Omega PX01C0-7.5, 0.1% linear accuracy). A thermostated water bath circulated water

*Correspondence: saca@mbari.org

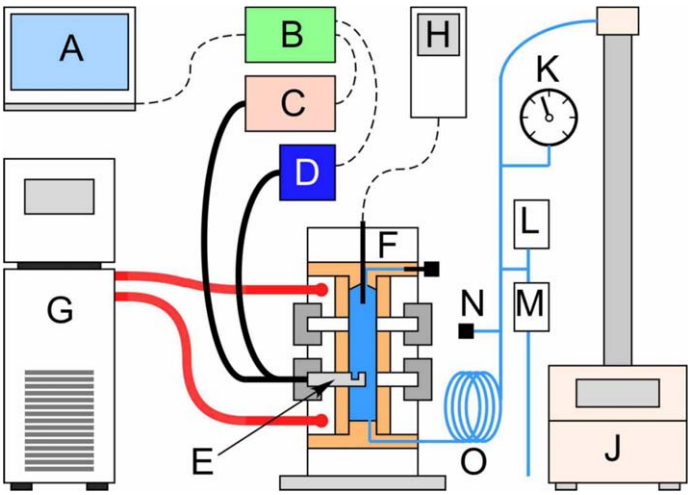

Fig. 1. A computer (A) communicates with a custom MSC (B) that controls the Heraeus UV Fiberlight (C) and the Zeiss MMS UV spectrometer (D). These are connected with a bifurcated fiber (Heraeus 600 μm UV solarization resistant) to the MBARI optimized optical immersion probe (E). The probe is mounted in a PEEK-lined titanium pressure chamber (F) that is temperature controlled by a Neslab programmable temperature bath (G). The chamber temperature is measured with an NIST calibrated thermistor (H). Pressure is controlled by an ISCO high-pressure pump (J) and monitored by a visual pressure gauge (K), an NIST calibrated electronic pressure gauge (L) and safety pressure relief valve (M). A T-fitting (N) is used to flush a spool of stainless steel tubing (152 cm $\times$ 1.75 mm i.d.) and PEEK tubing (152 cm $\times$ 0.8 mm i.d.) (O) with the same fluid as in the pressure chamber to maintain fluid composition during pressure cycling.

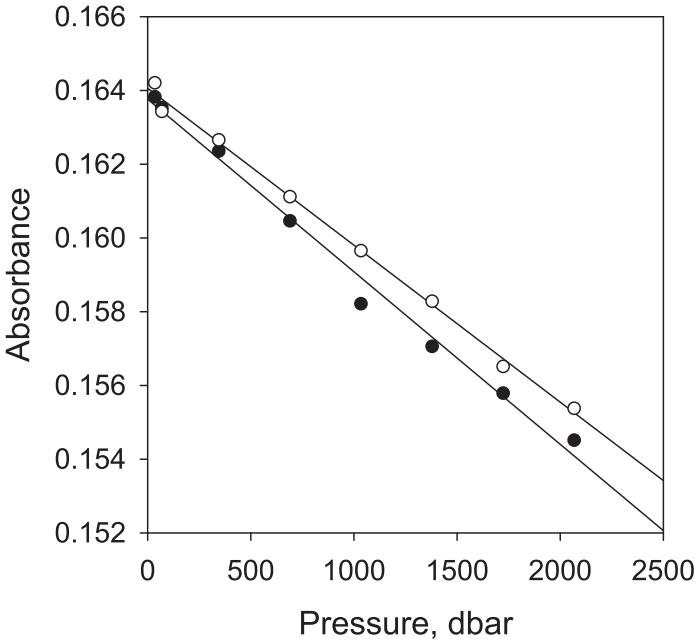

Fig. 2. The decompression baseline corrected absorbance at 217 nm of 840 μM NaBr solution (black circles) and low nutrient seawater (white circles) normalized to $S = 34.2$ at a sample temperature of 15°C. The absorbance spectra were baseline corrected by subtracting a linear regression of the uncorrected absorbances vs. wavelength fitted over the range 244–260 nm. The solid lines are the linear regressions of absorbance vs. pressure.

through channels bored in the body of the titanium vessel. Temperature in the pressure vessel was measured with a National Institute of Standards and Technology (NIST) certified YSI 4600 sensor. The calibration chamber was placed on top of a magnetic stirrer and a small stir bar was inserted in the chamber to mix the solution during experiments.

The volume of the apparatus contacting sample (pump cylinder, tubing, pressure chamber) was first flushed with freshly dispensed Millipore Milli-Q deionized water at least five times and then the standard solution was flushed from the T-connection (Fig. 1) to the chamber inlet. Care must be taken to minimize contamination from any plasticizers which have a signal in the UV wavelengths. Tygon tubing from the Milli-Q dispenser was replaced with Pharma-80 tubing, which has been found to have a lower effect on UV absorbance, and the deionized water was kept in acid cleaned glass bottles. The pressure chamber itself was flushed by manually filling and emptying the pressure chamber at least five times with the standard solution. The deionized water reference absorbances were calculated based on the last scan taken before flushing the apparatus with the seawater or bromide solution.

The spectrophotometer consisted of a Heraeus Fiberlight deuterium light source and a Zeiss MMS Series photodiode array spectrometer optimized for the UV. A fiber-optically coupled immersion probe from Equitech International, of the type used in ISUS nitrate sensors, was inserted into the calibration chamber with a pressure retaining seal. The MBARI optimized optical immersion probe was designed to withstand 4000 dbar pressure. The sensor was controlled by a microcontroller based system designed at MBARI (Multi-Sensor Controller [MSC]) and used to operate ISUS nitrate sensors and Deep-Sea DuraFET pH sensors in profiling floats. The spectral data was logged every 2 min.

The UV spectra of freshly dispensed deionized water (Millipore Milli-Q), surface seawater, or 840 μM NaBr (Fisher Scientific ACS reagent grade) were measured as functions of temperature and pressure. The low nutrient seawater was collected off the coast of Mexico in acid cleaned glass jugs. Nitrate concentration in this seawater was determined to be < 0.1 μM using standard methods (Sakamoto et al. 1990) and salinity was determined by conductivity. Care was taken to prevent contamination of these solutions from the plasticizers and materials in Tygon, Buna O-rings, and other plastics.

Assessment

Calculations of nitrate concentrations use wavelengths in the range 217–240 nm with the highest absorbance occurring at 217 nm. The UV light absorbance of seawater at 217 nm normalized to the sample salinity $S = 34.2$ is plotted vs. pressure in Fig. 2. The absorbance decreases linearly with pressure. Also shown is the absorbance at the same

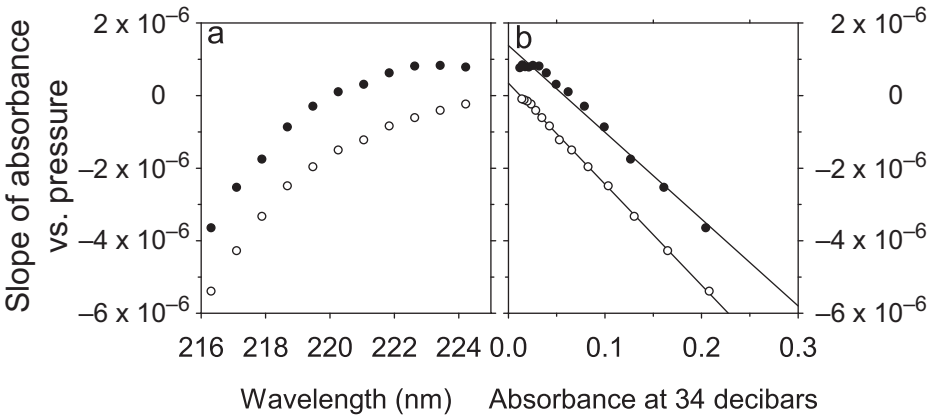

Fig. 3. The compression values (black circles) and decompression values (white circles) for the slope of the seawater absorbance vs. pressure (dbar) plotted vs. (**a**) wavelength, and (**b**) the respective absorbance value at 34 dbar pressure for low nutrient seawater at 15°C. The solid lines are the linear regressions of these values from 216.3 nm to 224.2 nm.

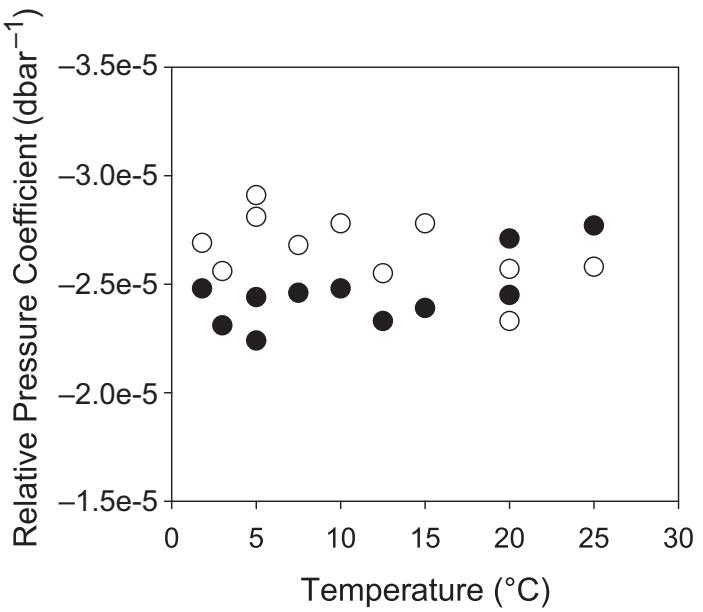

Fig. 4. The relative pressure coefficient plotted vs. temperature. The compression (34 up to 2068 dbar) values are shown as black circles and the decompression (2068 back to 34 dbar) values are shown as open circles.

wavelength of 840 μM NaBr solution, which corresponds to the bromide concentration in the same salinity seawater (Morris and Riley 1966). The absorbance of the 840 μM NaBr solution has a slope vs. pressure of $-(4.68 \pm 0.19) \times 10^{-6}$ absorbance dbar^{-1} ($n = 8$, $r^2 = 0.990$, 95% CI), while the $S = 34.2$ low nutrient seawater has a similar slope of $-(4.26 \pm 0.10) \times 10^{-6}$ absorbance dbar^{-1} ($n = 8$, $r^2 = 0.996$, 95% CI). The decreases in absorbance with increasing pressure for NaBr and seawater solutions with similar Br^- concentrations are not different at the 95% confidence level (*t*-test on slopes $p = 0.07$). The decrease in seawater UV absorption with increasing pressure is due primarily to a decrease in the light absorption of bromide ion.

The slope of the change in absorbance with pressure (absorbance dbar^{-1}) vs. wavelength for low nutrient seawater at 15°C is plotted in Fig. 3a. The slopes are more negative at the lower wavelengths where the absorbances are larger and level out with decreasing absorbance.

In order to determine if the pressure coefficient is wavelength dependent, the pressure coefficient at each wavelength (absorbance dbar^{-1}) was plotted vs. the absorbance at the starting pressure (34 dbar) at wavelengths from 216.3 to 224.2 in Fig. 3b. The pressure coefficients are linearly related to the absorbance measured at low pressure. The compression (34 up to 2068 dbar) regression has $y = -2.52 \times 10^{-5}\, x + 4.50 \times 10^{-8}$ ($r^2 = 0.995$, 95% CI) and the subsequent decompression (2068 to 34 dbar) regression has $y = -2.79 \times 10^{-5}\, x + 1.01 \times 10^{-8}$ ($r^2 = 0.999$, 95% CI). There was an overall slight increase in absorbance over time during the course of each experiment cycle that produces a nonzero intercept. This absorbance increase was largest on the compression cycle and may be related to a UV absorbing contaminant from the pump that entered the pressure chamber as the solution was compressed. It has a much smaller bias on the decompression cycles, with values near zero when the data is plotted vs. the lowest pressure absorbance on the decompression cycle (Fig. 3). Our interest is the slope of the line, which is independent of compression or decompression. We refer to this slope as the relative pressure coefficient of the absorbance with units dbar^{-1} (absorbance dbar^{-1} absorbance^{-1} = dbar^{-1}). The constant slope indicates that the relative pressure coefficient is the same at each wavelength.

Eleven experiments were run at different temperatures and the values of the relative pressure coefficient are plotted in Fig. 4 vs. temperature. There is no significant trend in the data vs. temperature. The average of all the seawater data is $-(2.6 \pm 0.2) \times 10^{-5}$ dbar^{-1} (1 SD). As a result, we treat the relative pressure coefficient as wavelength and temperature independent.

The computation of nitrate concentration in seawater, using the algorithm reported by Sakamoto et al. (2009) requires that the absorbance spectrum of seawater (1 cm

pathlength) be estimated from the observed salinity and temperature for each sample

$$A_{SW,\lambda} = E_{SW,\lambda,T} * S \quad (1)$$

where A is absorbance at wavelength λ, $E_{SW,\lambda}$ is the absorptivity of seawater over 1 cm, S is the salinity, and T is temperature. Values of $E_{SW,\lambda,T\mathrm{Cal}}$ are determined in the laboratory for each UV nitrate sensor by measuring the absorbance of a low nitrate seawater sample at a calibration temperature, T_{Cal}, and dividing the observed baseline corrected (240–260 nm) absorbance at each wavelength by salinity. During a laboratory calibration, the solutions are pumped against a 28 dbar backpressure regulator to eliminate air bubbles in the sample stream. The values of $E_{SW,\lambda,T}$ are then computed as described by Sakamoto et al. (2009). The existence of a pressure coefficient that is wavelength and temperature independent means that Eq. 1 must be rewritten as

$$A_{SW,\lambda,\mathrm{pressure}} = E_{SW,\lambda,T,\mathrm{pressure}} * S \quad (2)$$

where

$$E_{SW,\lambda,T,\mathrm{pressure}} = E_{SW,\lambda,T,1\,\mathrm{dbar}} * (1 - 0.026 * \mathrm{Pressure\,(dbar)}/1000) \quad (3)$$

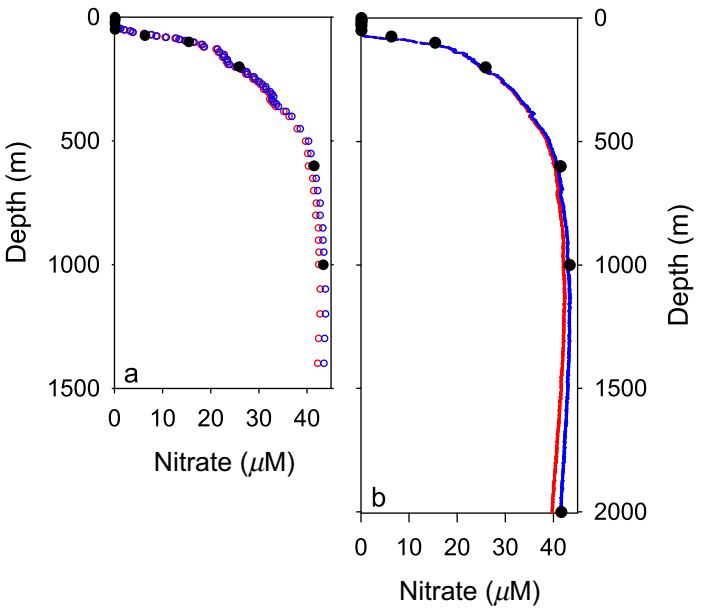

Fig. 5. (**a**) In situ nitrate data from a profiling float (#8501CalCurrent) off the central California coast. The calculated nitrate concentrations without pressure correction of the bromide absorbance (red circles) and with pressure correction (blue circles) and the discrete nitrate concentrations from the accompanying bottle cast (black circles) are shown vs. depth. (**b**) In situ nitrate data from an ISUS sensor on a CTD-Rosette cast at the same location. The calculated nitrate concentrations without pressure correction of the bromide absorbance (red line) and with pressure correction (blue line) and the discrete nitrate concentrations from the accompanying bottle cast (black circles) are shown vs. depth.

Without taking into account the pressure dependence, the expected absorbance due to sea salts at high pressure will be too high. The sample absorbance corrected by then removing the sea salt absorbance will be artificially too low and the nitrate values calculated from the corrected spectra will also be biased low at high pressure.

We conducted a test cruise about 280 km off the coast of central California on the R/V *Rachel Carson* in February 2016 and the results can be used to assess the magnitude of the bias in estimated nitrate concentration. We deployed a profiling float (#8501CalCurrent) and Fig. 5a shows a nitrate profile computed with and without the pressure corrections from this profiling float and the discrete nitrate values from the closest cast to the deployment.

To further test the pressure correction effect on the bromide absorption, during this cruise, we also deployed an ISUS on the conductivity-temperature-depth (CTD) rosette

Table 1. Summary data from six casts off the central California coast. The difference between the calculated nitrate concentrations with and without correction for the pressure effect on the bromide absorbance gives the magnitude of the correction that needs to be applied.

Cast #	Depth (m)	Temperature (°C)	Salinity	Nitrate pressure corrected (μM)	Nitrate no pressure correction (μM)	Difference
1	1000	3.95	34.44	43.30	42.34	0.96
2	1000	3.89	34.44	42.97	42.02	0.95
2	2000	2.01	34.61	41.62	39.80	1.82
3	1000	3.76	34.44	43.17	42.22	0.95
3	2000	1.98	34.61	41.27	39.44	1.83
4	1000	3.92	34.44	42.85	41.90	0.95
4	2000	1.96	34.61	41.01	39.19	1.82
5	1000	3.87	34.44	43.11	42.15	0.96
5	2000	2.01	34.61	41.44	39.61	1.83
6	1000	3.86	34.45	42.36	41.41	0.95
6	2000	1.95	34.62	40.53	38.71	1.82

and collected discrete samples for nutrient analysis onshore. The first cast went to 1000 m and then five more casts were done to 2000 m. Figure 5b shows a nitrate profile computed with and without the pressure correction and the associated discrete nitrate values. The mean and standard deviation of 10 replicate measurements at the deepest depth of this cast (2025 m) is 41.41 ± 0.07 μM nitrate.

Table 1 summarizes the results of the comparisons at 1000 m and 2000 m for all the CTD casts. The average error that would be introduced by neglecting the pressure effect would be about 0.95 ± 0.005 μM nitrate at 1000 dbar and 1.82 ± 0.005 μM at 2000 m. Because the salinity of deep seawater is nearly constant at 35, the error introduced by neglect of this effect also has a nearly constant influence on the computed nitrate throughout the world ocean at a given pressure. The correction amounts to an error of around 0.95 μM nitrate at 1000 dbar.

Comments and recommendations

The pressure dependence of the bromide extinction coefficient in seawater has been measured in the laboratory. A distinct pressure coefficient that is consistent with the observations of Pasqueron de Fommervault et al. (2015) was found. For calculations at high pressures, the pressure dependence of 2.6% decrease in the E_{SW} values per 1000 dbar pressure should be included in the calculations as well as the temperature corrections for seawater. This shifts computed nitrate concentrations at 1000 dbar by 0.95 μM and, because salinity is relatively constant throughout the deep ocean, this correction is nearly constant for all areas.

The new pressure and temperature chamber used in these experiments allowed determination of the pressure dependence of the bromide absorbance. The temperature control of the solutions in this chamber will allow for checking and perhaps refining the temperature coefficients of the bromide absorption at higher and lower temperatures than were previously possible.

References

Aubert, A. H., and L. Breuer. 2016. New seasonal shift in in-stream diurnal nitrate cycles identified by mining high-frequency data. PLoS One **11**: e0153138. doi:10.1371/journal.pone.0153138

Collins, J. R., P. A. Raymond, W. F. Bohlen, and M. M. Howard-Strobel. 2013. Estimates of new and total productivity in central Long Island Sound from in situ measurements of nitrate and dissolved oxygen. Estuaries Coast. **36**: 74–97. doi:10.1007/s12237-012-9860-5

D'Ortenzio, F., and others. 2014. Observing mixed layer depth, nitrate and chlorophyll concentrations in the northwestern Mediterranean: A combined satellite and NO_3 profiling floats experiment. Geophys. Res. Lett. **41**: 6443–6451. doi:10.1002/2014GL061020

Frank, C., D. Meier, D. Voß, and O. Zielinski. 2014. Computation of nitrate concentrations in coastal waters using an in situ ultraviolet spectrophotometer: Behavior of different computation methods in a case study a steep salinity gradient in the southern North Sea. Methods Oceanogr. **9**: 34–43. doi:10.1016/j.mio.2014.09.002

Harvey, J., Y. Zhang, and J. Ryan. 2012. AUVs for ecological studies of marine plankton communities. Sea Technol. **53**: 51–54.

Johnson, K. S., and L. J. Coletti. 2002. In situ ultraviolet spectrophotometry for high resolution and long-term monitoring of nitrate, bromide and bisulfide in the ocean. Deep-Sea Res. Part I Oceanogr. Res. Pap. **49**: 1291–1305. doi:10.1016/S0967-0637(02)00020-1

Johnson, K. S., and J. A. Needoba. 2008. Mapping the spatial variability of plankton metabolism using nitrate and oxygen sensors on an autonomous underwater vehicle. Limnol. Oceanogr. **53**: 2237–2250. doi:10.4319/lo.2008.53.5_part_2.2237

Johnson, K. S., S. C. Riser, and D. M. Karl. 2010. Nitrate supply from deep to near-surface waters of the North Pacific subtropical gyre. Nature **465**: 1062–1065. doi:10.1038/nature09170

Johnson, K. S., L. J. Coletti, H. W. Jannasch, C. M. Sakamoto, D. D. Swift, and S. C. Riser. 2013. Long-term nitrate measurements in the ocean using the in situ ultraviolet spectrophotometer: Sensor integration into the APEX profiling float. J. Atmos. Ocean. Technol. **30**: 1854–1866. doi:10.1175/JTECH-D-12-00221.1

Johnson, K. S., and others. 2017. Biogeochemical sensor performance in the SOCCOM profiling float array. J. Geophys. Res. Oceans. **122**, doi:10.1002/2017JC012838

MacIntyre, G., and others. 2009. ISUS/SUNA nitrate measurements in networked ocean observing systems, p. 1–7. *In* OCEANS 2009, MTS/IEEE Biloxi-Marine Technology for Our Future: Global and Local Challenges. IEEE.

Morris, A. W., and J. P. Riley. 1966. The bromide/chlorinity and sulphate/chlorinity ratio in sea water. Deep-Sea Res. Oceanogr. Abstr. **13**: 699–705. doi:10.1016/0011-7471(66)90601-2

Pasqueron de Fommervault, O., and others. 2015. Seasonal variability of nutrient concentrations in the Mediterranean Sea: Contribution of Bio-Argo floats. J. Geophys. Res. Oceans **120**: 8528–8550. doi:10.1002/2015JC011103

Pellerin, B. A., B. D. Downing, C. Kendall, R. A. Dahlgren, T. E. C. Kraus, J. Saraceno, R. G. M. Spencer, and B. A. Bergamaschi. 2009. Assessing the sources and magnitude of diurnal nitrate variability in the San Joaquin River (California) with an in situ optical nitrate sensor and dual nitrate isotopes. Freshw. Biol. **54**: 376–387. doi:10.1111/j.1365-2427.200802111.x

Sakamoto, C. M., G. E. Friederich, and L. A. Codispoti. 1990. MBARI procedures for automated nutrient analyses using a modified Alpkem Series 300 Rapid Flow Analyzer, p. 87. Monterey Bay Aquarium Research Institute Tech. Rep 90-2.

Sakamoto, C. M., K. S. Johnson, and L. J. Coletti. 2009. Improved algorithm for the computation of nitrate concentrations in seawater using an in situ ultraviolet spectrophotometer. Limnol. Oceanogr.: Methods **7**: 132–143. doi:10.4319/lom.2009.7.132

Woodgate, R. A., K. M. Stafford, and F. G. Prahl. 2015. A synthesis of year-round interdisciplinary mooring measurements in the Bering Strait (1990–2014) and the RUSALCA years (2004–2011). Oceanography **28**: 46–67. doi:10.5670/oceanog.2015.57

Zielinski, O., D. Voß, B. Saworski, B. Fiedler, and A. Körtzinger. 2011. Computation of nitrate concentrations in turbid coastal waters using an in situ ultraviolet spectrophotometer. J. Sea Res. **65**: 456–460. doi:10.1016/j.seares.2011.04.002

Acknowledgments

Thanks to M. Blum for assistance with the discrete nutrient analyses, and V. Elrod and J. Plant for assistance on the cruise and thanks also to the crew of the Research Vessel Rachel Carson. This work was supported by the David and Lucile Packard Foundation to the Monterey Bay Aquarium Research Institute.

Conflict of Interest

None declared.

Submitted 13 March 2017
Revised 06 July 2017
Accepted 23 August 2017

Associate editor: Gregory Cutter